AGU PUBLICATIONS

Geochemistry, Geophysics, Geosystems

RESEARCH ARTICLE
10.1002/2015GC005795

Multiparametric study of the February–April 2013 paroxysmal phase of Mt. Etna New South-East crater

Letizia Spampinato[1], Mariangela Sciotto[1], Andrea Cannata[1], Flavio Cannavò[1], Alessandro La Spina[1], Mimmo Palano[1], Giuseppe G. Salerno[1], Eugenio Privitera[1], and Tommaso Caltabiano[1]

[1]Istituto Nazionale di Geofisica e Vulcanologia, Sezione di Catania-Osservatorio Etneo, Catania, Italy

Key Points:
- This study contributes to the understanding of Etna eruptive behavior since 2011
- The source and mechanism of the explosive sequence were investigated
- Etna's lava fountains were investigated by a multidisciplinary approach

Correspondence to:
L. Spampinato,
letizia.spampinato@ingv.it

Citation:
Spampinato, L., M. Sciotto, A. Cannata, F. Cannavò, A. La Spina, M. Palano, G. G. Salerno, E. Privitera, and T. Caltabiano (2015), Multiparametric study of the February–April 2013 paroxysmal phase of Mt. Etna New South-East crater, *Geochem. Geophys. Geosyst.*, *16*, 1932–1949, doi:10.1002/2015GC005795.

Received 26 FEB 2015
Accepted 15 MAY 2015
Accepted article online 21 MAY 2015
Published online 26 JUN 2015

Abstract Between January 2011 and April 2013, Mt. Etna's eruptive activity consisted of episodic intra-crater strombolian explosions and paroxysms from Bocca Nuova, Voragine, and the New South-East (NSEC) summit craters, respectively. Eruptions from NSEC consisted of initial increasing strombolian activity and lava flow output, passing to short-lasting lava fountaining. In this study we present seismic, infrasound, radiometric, plume SO_2 and HCl fluxes and geodetic data collected by the INGV monitoring system between May 2012 and April 2013. The multiparametric approach enabled characterization of NSEC eruptive activity at both daily and monthly time scales and tracking of magma movement within Mt. Etna's plumbing system. While seismic, infrasound and radiometric signals give insight on the energy and features of the 13 paroxysms fed by NSEC, SO_2 and halogen fluxes shed light on the likely mechanisms triggering the eruptive phenomena. GPS data provided clear evidence of pressurization of Mt. Etna's plumbing system from May 2012 to middle February 2013 and depressurization during the February–April 2013 eruptive activity. Taking into account geochemical data, we propose that the paroxysms' sequence represented the climax of a waxing-waning phase of degassing that had started as early as December 2012, and eventually ended in April 2013. Integration of the multidisciplinary observations suggests that the February–April 2013 eruptive activity reflects a phase of release of a volatile-rich batch of magma that had been stored in the shallow volcano plumbing system at least 4 months before, and with the majority of gas released between February and March 2013.

1. Introduction

Mt. Etna is an open-vent basaltic volcano (~3300 m a.s.l.) located in the eastern area of Sicily (South Italy; inset in Figure 1a, left) and characterized by quiescent degassing and frequent eruptions either from the summit area or the flanks [e.g., *Rittmann*, 1973; *Mulargia et al.*, 1985; *Branca and Del Carlo*, 2005]. Eruptive activity ranges from moderate lava effusion [e.g., *Burton et al.*, 2005] to explosive activity of variable intensity, including lava fountaining, from eruptive fissures [e.g., *Acocella and Neri*, 2003; *Andronico et al.*, 2005; *Spampinato et al.*, 2008] or the volcano summit craters [e.g., *Alparone et al.*, 2003; *Behncke et al.*, 2006; *Andronico and Corsaro*, 2011].

Lava fountains are spectacular manifestations of active volcanism, characterized by incandescent lava jets of heights from tens-to-hundreds of meters that can last from minutes to days [e.g., *Wilson and Head*, 1981, 2001; *Oppenheimer and Francis*, 1997; *Parfitt*, 1998]. The nature and conditions leading to lava fountains have been widely discussed using methodologies spanning from ground-based observations to satellite imagery and laboratory experiments [e.g., *Jaupart and Vergniolle*, 1988, 1989; *Alparone et al.*, 2003; *Allard et al.*, 2005; *Friedman et al.*, 2006; *Spampinato et al.*, 2008; *Ganci et al.*, 2012; *Gouhier et al.*, 2012; *La Spina et al.*, 2015]. The rapidity, with which lava fountains develop, and the high energy released have forced the volcanology community to make efforts to better understand this eruptive regime [e.g., *Endo et al.*, 1988; *Hayashi et al.*, 1992; *Mangan and Cashman*, 1996; *Parfitt*, 2004; *Vergniolle and Ripepe*, 2008; *Staudacher et al.*, 2009; *Stovall et al.*, 2011; *Bonaccorso et al.*, 2014]. Recently at Mt. Etna, the need to predict, characterize and track the occurrence of lava fountains for civil protection purposes has promoted multidisciplinary approaches for monitoring and investigation of lava fountaining from the summit craters, and especially of the most recent sequences fed by a new crater starting in January 2011 [e.g., *Langer et al.*, 2009; *Calvari et al.*, 2011; *Bonaccorso et al.*, 2013, 2014; *Patanè et al.*, 2013].

The new crater started developing at the foot of the eastern flank of the South-East summit crater (SEC) of Mt. Etna in late 2009 [*La Spina and Salerno*, 2009; *Calvari et al.*, 2011; *Patanè et al.*, 2013] (inset in Figure 1a, right).

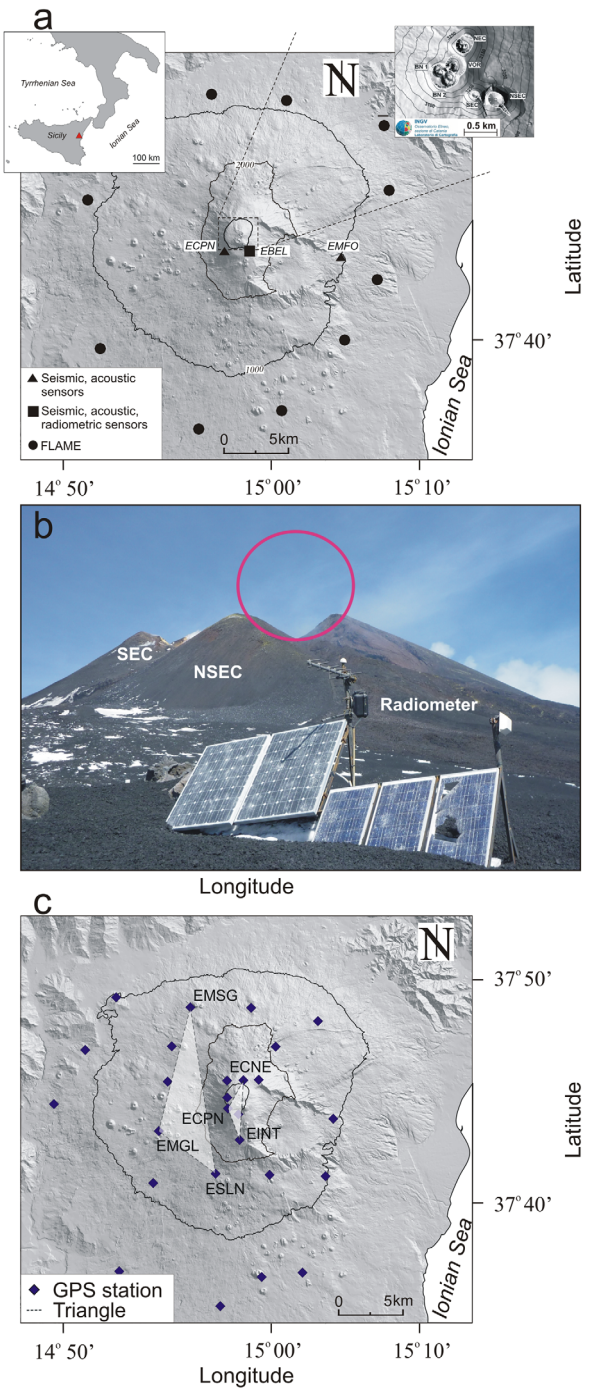

Figure 1. (a) Shaded relief map of Mt. Etna volcano showing the location of the seismic, acoustic and radiometric stations used for this study, and the geometry of the FLAME UV scanner network. The inset on the left shows the geographic location of Mt. Etna and the inset on the right is a magnification of the volcano summit area. (b) Photograph showing EBEL integrated station, the New South-East crater (NSEC) with the South-East crater (SEC) at the back, and the radiometer FOV (area delimited by the pink circle). (c) Stations of the permanent GPS network analyzed in this study; summit and intermediate altitude triangles are also shown.

Initially a pit crater, a new cone rapidly grew due to intense episodic eruptive activity fed between 2011 and 2013 [*Calvari et al.*, 2011; *Bonaccorso et al.*, 2013; *Behncke et al.*, 2014]. Overlapping of lava flows and pyroclasts allowed the hereinafter named New South-East Crater (NSEC) to reach sizes comparable with the nearby SEC [*Behncke et al.*, 2014]. While lava flows emplaced eastward, explosive activity, consisting of initial strombolian explosions evolving into lava fountains, produced eruptive columns and copious ash fallouts that frequently forced the closure of the Catania airport [*Calvari et al.*, 2011; *Ganci et al.*, 2012].

Paroxysms at NSEC stopped in spring 2012 and renewed in the second half of February 2013 lasting until the end of April 2013. In this paper, we report on this ~2 month paroxysmal phase by integration of geochemical, seismic, infrasound, thermal and geodetic data recorded by the Istituto Nazionale di Geofisica e Vulcanologia, Osservatorio Etneo (INGV-OE) permanent networks and portable Fourier Transform InfraRed (FTIR) spectrometers. For this study, we focus on data collected between May 2012 and April 2013 with particular emphasis on geophysical and geochemical observations recorded from February to April 2013. The synoptic outlook allows us to characterize each of the February–April 2013 paroxysms and assess the likely mechanisms for the renewed activity at NSEC.

2. NSEC Eruptive Activity

2.1. Eruptive Activity Between May and December 2012

Following the last lava fountain of April 2012 and until the first half of November 2012, the activity of NSEC included weak degassing mainly from the fumaroles located along the crater rim [e.g., *INGV-OE Internal Report*, 2012a, 2012b] and episodes of ash emission from the morphological depression between SEC and NSEC [e.g., *INGV-OE Internal Report*, 2012c, 2012d]. At the end of November 2012, NSEC activity became focused inside the crater with incandescence due to emission of high temperature gases [e.g., *INGV-OE Internal Report*, 2012e, 2012f]. In December, the degassing style changed to intermittent and dense gas release, and poor emissions of fine volcanic material [e.g., *INGV-OE Internal Report*, 2012g].

It is noteworthy that between July and October 2012, the Bocca Nuova (BN) summit crater also fed eruptive activity from one of the two pits (BN1 in Figure 1a, top-right corner). Continuous intracrater strombolian explosions and lava output were recorded from 2 July to the end of August, and on 2 and 18 October 2012. Eruptive activity formed an intracrater cone due to the superimposition of pyroclastic products and lava flows [e.g., *INGV-OE Internal Report*, 2012h].

2.2. Eruptive Activity Between January and April 2013

In 2013 the INGV-OE monitoring networks showed renewal of the eruptive activity at NSEC [*INGV-OE Internal Report*, 2013a]. In January, sporadic low intensity strombolian explosions interspaced by ash emissions were observed [*INGV-OE Internal Report*, 2013a, 2013b, 2013c, 2013d]. In February, the intensity of explosive activity increased, though it was initially confined within NSEC, and displayed discontinuous pulsating incandescence [*INGV-OE Internal Report*, 2013e, 2013f]. From 15 to 17 February, the eruptive activity intensified with continuous explosions ejecting fresh scoriae outside the crater rim [*INGV-OE Internal Report*, 2013f]. After the evening of 18 February, NSEC activity resumed leading to the paroxysmal phase that eventually ended late in April 2013 [*INGV-OE Internal Report*, 2013g]. Overall, between 19 February and 27 April 2013, NSEC fed 13 paroxysmal episodes [*INGV-OE Internal Report*, 2013g]. Each of the episodes was characterized by strombolian activity growing in intensity, lava flow effusion, and transition from discrete explosions to the continuous gas and lava jetting typical of lava fountaining [e.g., *Parfitt*, 2004; *INGV-OE Internal Report*, 2013g]. Between the 4 months of observations, the BN and Voragine (VOR) summit craters were also sporadically active. In particular, BN fed intracrater strombolian explosions on 3, 9, 14, 16, 18, and 28–30 January, 8–9 and 27 February, and 3, 4, and 17 March [*INGV Internal Report*, 2013a, 2013d, 2013e, 2013h, 2013i]. VOR produced intra-crater strombolian activity on 27 February and 1, 3, and 9 March, and ash emissions on 3, 5, 8, and 17 March 2013 [*INGV Internal Report*, 2013h].

3. Methodology and Results

3.1. Seismic and Infrasound Signals

The seismic and infrasonic investigations were performed on the signals recorded by EBEL and EMFO stations for the intervals between May 2012 to February 2013 and February–April 2013, respectively (Figure 1a). An additional station—ECPN—was used for the entire period to study the long period (LP) events (Figure 1a). EBEL, EMFO, and ECPN are sited on Mt. Etna's eastern and south-eastern flanks at elevations of ~2850, 1200, and 3040 m (a.s.l.), respectively, and distances from NSEC of ~1, 7.4, and 1.4 km, respectively (Figure 1a). ECPN is "historically" considered the reference station for the LP event analysis at Mt. Etna because of its proximity to the most active LP source located below BN [e.g., *Cannata et al*., 2009a; *Patanè et al*., 2008, 2013]. Switching from EBEL to EMFO for the study of NSEC was necessary due to the destruction of the former by lava flows fed by the 28 February 2013 paroxysm. The choice of using data from EBEL is based on its proximity to NSEC and to the high signal-to-noise ratio. The equipment of the stations consist of broadband sensors (40 s cutoff period) equipped with three-component Trillium seismometers (Nanometrics) sampling data at 100 Hz. The infrasonic microphones are G.R.A.S. 40AN acoustic sensors with flat response in the frequency range of 0.3–20 Hz and sensitivity of 50 $mV \times Pa^{-1}$, acquiring acoustic signals at a frequency of 50 Hz. Seismic and infrasound amplitudes were obtained by calculating a RMS (root-mean-square) envelope on 10 min-long windows (Figures 2a, 2b, 3a, and 3b). In order to calculate the RMS values both seismic and infrasonic signals were filtered in the 0.5–5.5 Hz band, which contains most of the seismic and infrasonic volcano energy [e.g., *Cannata et al*., 2013].

The seismic signal recorded at the summit stations of Mt. Etna is dominated by volcanic tremor, whose source mechanism is generally associated with fluid dynamics in the volcano plumbing systems [e.g., *Chouet*, 1996]. The most important aspects of volcanic tremor at Mt. Etna are its continuity in time, and its close relationship to changes in eruptive activity, highlighted by variations in amplitude, spectral content, wavefield features, and source location [e.g., *Cannata et al*., 2013]. While the seismic RMS is mainly dominated by temporal changes of the volcanic tremor energy (except for some peaks caused by volcano-tectonic earthquakes, tectonic earthquakes or energetic long period event swarm), the infrasonic RMS is modulated by both volcano-related signals and weather-dependent effects. The former are the so-called infrasonic events and tremor generated by degassing and explosive processes. The latter, and mainly the wind, causes broadband noise that is not easily removed. For this reason infrasonic RMS data, during noneruptive periods, show higher "background noise" than the seismic data. In our study, the maximum seismic

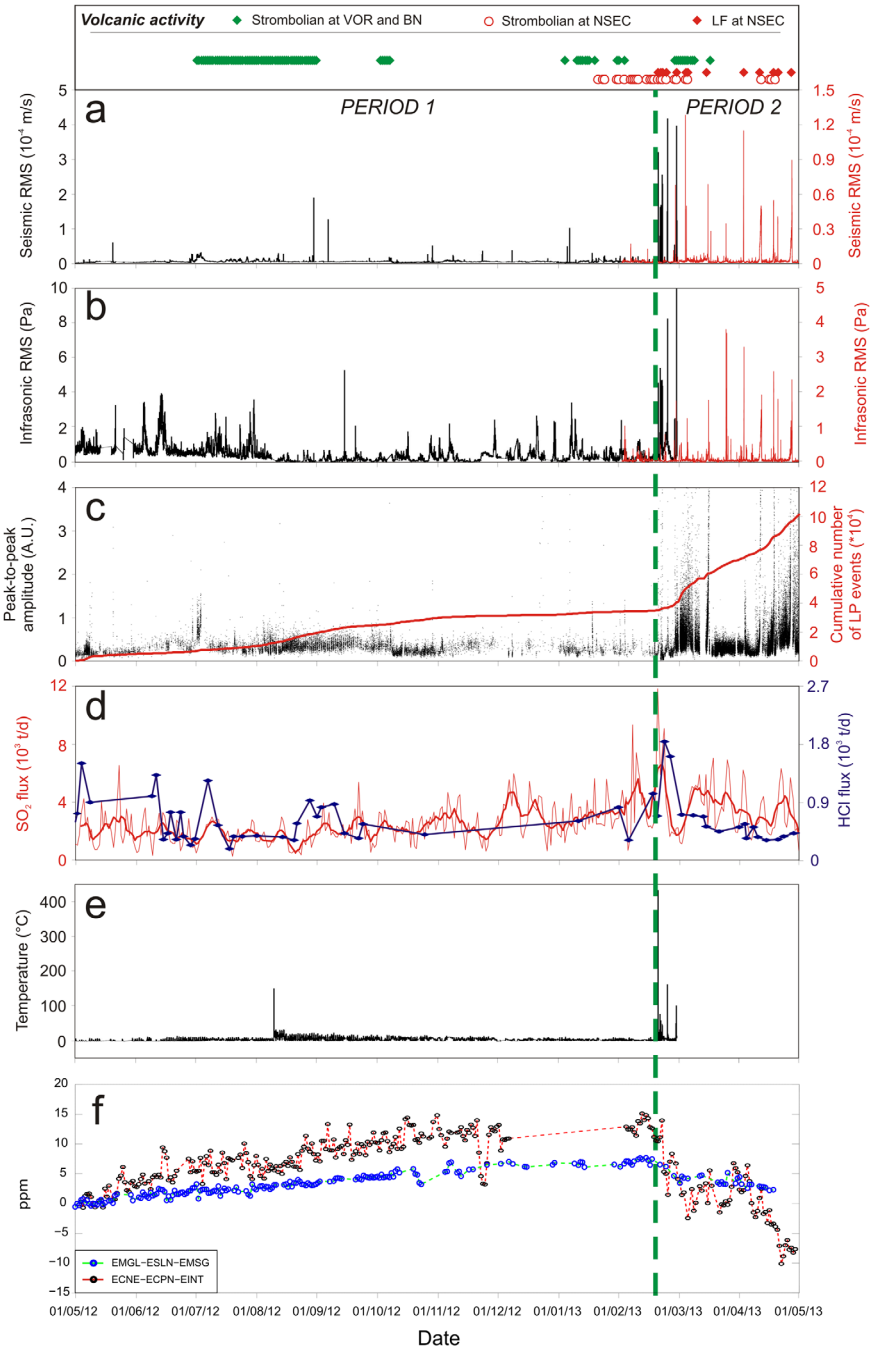

Figure 2. Temporal variation of (a) seismic RMS, (b) infrasonic RMS, (c) peak-to-peak amplitude (black dots) and cumulative daily number of LP events (red line), (d) SO_2 flux (thin red line) and HCl flux (blue line and dots), (e) radiometer RMS, and (f) areal variation of the two GPS triangles during 1 May 2012 – 30 April 2013. The black and red lines in Figures 2a and 2b correspond to the RMS of the vertical component of the seismic and infrasonic signal recorded by EBEL and EMFO stations, respectively. The thick red line in Figure 2d represents the SO_2 flux 7 day-moving average. The rectangle at top of Figure 2a indicates the main eruptive activity episodes taking place at the summit craters during the targeted time window. The green-dashed vertical line separates Period 1 (P1) from Period 2 (P2).

RMS values were reached during the paroxysmal episodes taking place from February to April 2013 (Figures 2a, 2b, 3a, and 3b). During paroxysms, both volcanic tremor and infrasound signal amplitude underwent gradual increases at the start of the strombolian activity and reached the highest amplitude values a few hours later with the development of the main lava fountaining phase. In particular, during the paroxysmal event climax, we observed that the discrete infrasonic events that generally accompany strombolian activity [e.g., *Vergniolle et al.*, 2004; *Vergniolle and Ripepe*, 2008], were replaced by continuous infrasonic tremor,

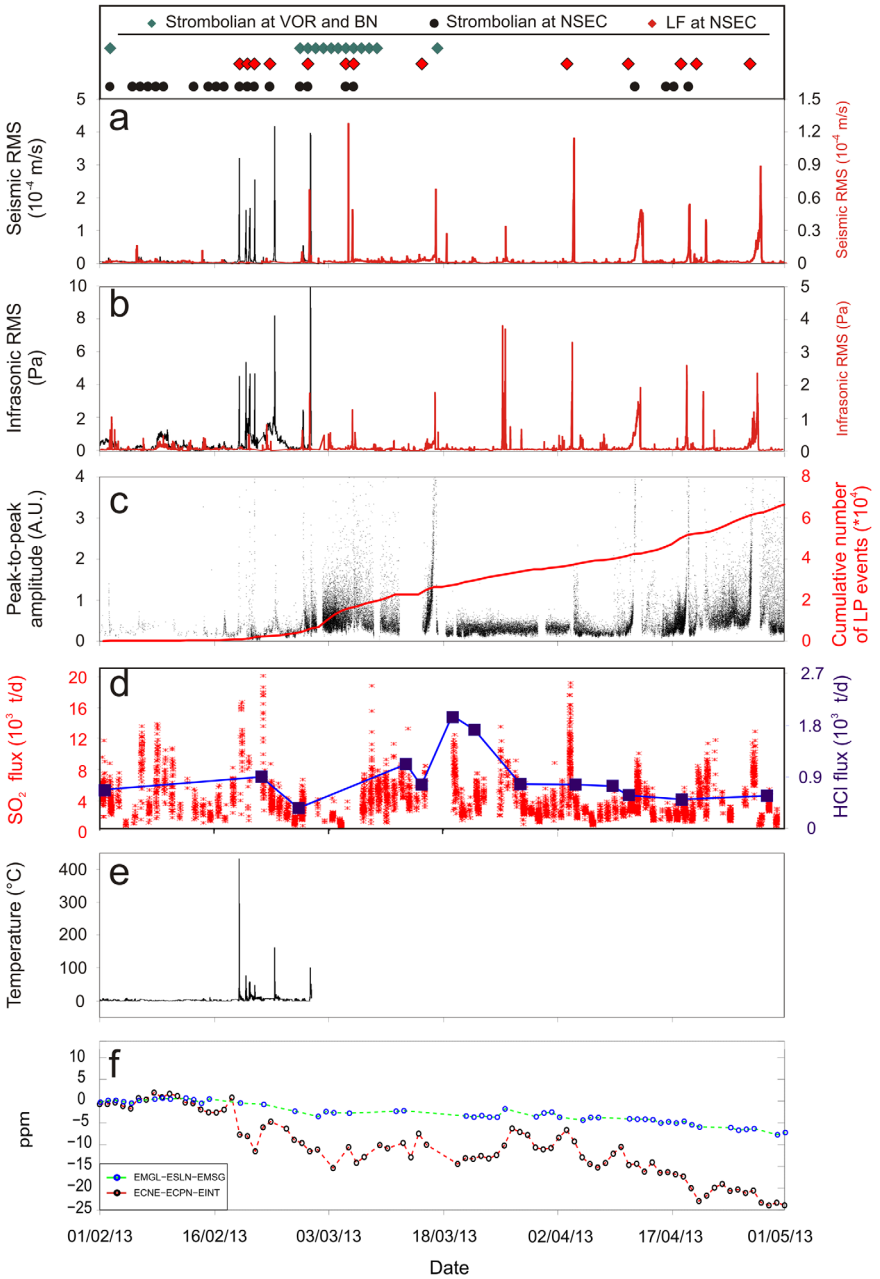

Figure 3. Magnification of Figure 2 showing the main features of the time window between 1 February and 30 April 2013.

observed during previous lava fountains at Mt. Etna [e.g., *Cannata et al.*, 2009b]. As previously observed at other volcanoes, during long lasting explosive eruptive episodes infrasound signal becomes continuous, preventing from pinpointing discrete events [e.g., *Caplan-Auerbach et al.*, 2010]. Smaller peaks occurred in both seismic and infrasound RMS amplitudes and were related to the BN and VOR volcanic activity that, occurred starting from January 2013.

Similarly to volcanic tremor, also the sources of LP events are related to the fluid dynamics in the volcano plumbing systems [e.g., *Chouet*, 1996]. An interesting aspect of the LP events recorded at Mt. Etna is the relation with volcanic activity, shown by changes in occurrence rate, energy, waveforms, spectral content, and/or source locations time-related to eruptive activities [e.g., *Patanè et al.*, 2008]. However, it is also worth noting that LP and VLP events are recorded at Mt. Etna even during noneruptive periods, and their occurrence is often not directly associated with any observable volcanic activity [e.g., *Cannata et al.*, 2009a].

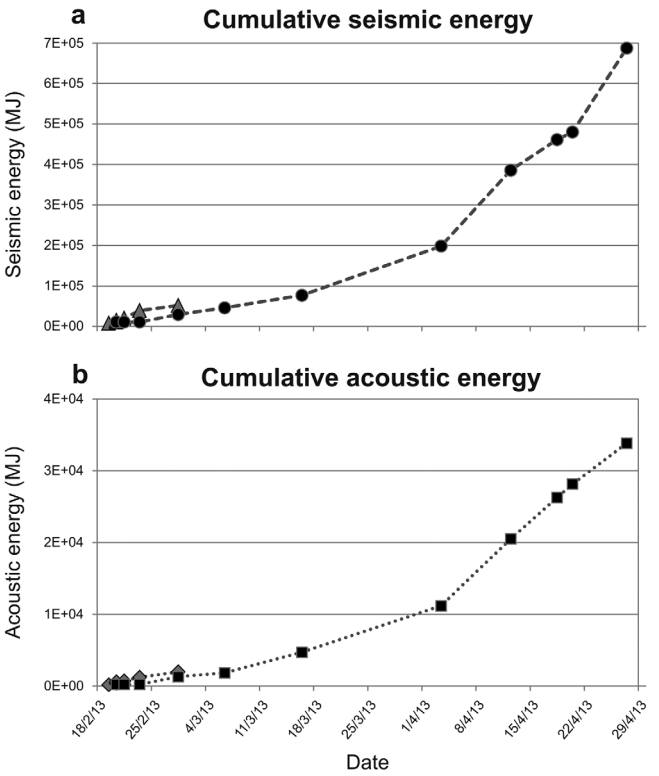

Figure 4. Cumulative (a) seismic and (b) acoustic energies (MJ), calculated at the EBEL and EMFO stations (grey solid diamonds and black solid squares, respectively), for the time window during which the lava fountain episodes occurred.

LP events were investigated by taking into account the cumulative daily number of events and their peak-to-peak amplitude calculated at ECPN station. Figures 2c and 3c show the sharp increase of both number and amplitude of LP events undergone at the end of February 2013. Mean daily LP events changed from ∼120 to ∼900 and mean amplitude values doubled.

In order to characterize each paroxysm, we also calculated the energy of the seismic and infrasonic signals recorded during the lava fountains (Figure 4). Energy estimation of acoustic and seismic signals has been used in literature to explore strombolian explosions, lava lake and ash emission type volcanic activity with the aim of investigating eruptive dynamics, and, by means of their comparison, gaining information about source depth and vent geometric features [e.g., *Johnson and Aster*, 2005; *Sciotto et al*., 2011; *Andronico et al*., 2013; *Richardson et al*., 2014]. Although the approach introduced by *Johnson and Aster* [2005] to estimate acoustic and seismic energy has been mainly applied to minor and discrete explosive episodes, recently it has been considered a good method for surveillance aims, both for local [*McNutt et al*., 2013] and long-range monitoring [*Fee et al*., 2010; *Dabrowa et al*., 2011] and to evaluate the strength of volcanic tremor during more explosive eruptive episodes [*West*, 2013; *McNutt et al*., 2013].

Here the seismic energy (Figure 4a) was evaluated assuming isotropic radiation at the top of a homogeneous half-space following the approach of *Johnson and Aster* [2005], and setting volcano density and P wave velocity equal to 2500 kg/m^3 and 1800 m/s, respectively (see *Sciotto et al*. [2011] and *Andronico et al*. [2013] for details about attenuation and site response chosen values). The recorded velocity included in the seismic energy equation [*Johnson and Aster*, 2005] was calculated as the resultant vector of the three-component traces at EBEL and EMFO. Similarly the acoustic energy radiated was calculated by integrating the excess pressure in space and time over a hemispherical surface [*Johnson and Aster*, 2005] and assuming the density of atmosphere and sound velocity of 0.9 kg/m^3 and 340 m/s, respectively (Figure 4b).

Lava fountain intervals were selected based on the seismic RMS time series and comprised the increasing patterns at the beginning of the episode, the paroxysmal phase and the decreasing patterns at the end of the episode (Table 1). Once the periods were selected, energies were calculated for each signal sample (representing 0.01 s and 0.02 s of seismic and infrasonic signals, respectively). Finally, one value of acoustic

Table 1. Lava Fountains From February to April 2013 With Their Start and End Times (GMT), Duration (h), and Seismic and Acoustic Energy (MJ) Calculated From Data of the EBEL and EMFO Stations

Lava Fountain Episode (Date)	Start (hh:mm)	End (hh:mm)	Duration (h)	Seismic Energy (MJ) at EMFO	Seismic Energy (MJ) at EBEL	Acoustic Energy (MJ) at EMFO	Acoustic Energy (MJ) at EBEL
19/02/13	00:00	06:00	6		7,91E+03		1.55E+02
20/02/13	22:00 (on 19/02/2013)	02:30	5.5		3.19E+03		1.75E+02
20/02/13	09:30	15:00	5.5	1.07E+04	3.94E+03	2.31E+02	2.49E+02
21/02/13	00:30	07:00	6.5		5.29E+03		1.43E+02
23/02/13	13:00	22:00	9		1.87E+04		5.08E+02
28/02/13	06:30	11:30	5	1.86E+04	1.28E+04	1.07E+03	7.47E+02
06/03/13	19:00 (on 05/03/2013)	00:30	5.5	1.66E+04		5.38E+02	
16/03/13	07:00	21:00	14	3.10E+04		2.88E+03	
03/04/13	07:30	16:00	9.5	1.21E+05		6.47E+03	
12/04/13	00:00 (on 11/04/2013)	12:30	24.5	1.87E+05		9.30E+03	
18/04/13	01:00	17:00	16	7.58E+04		5.78E+03	
20/04/13	07:00	19:00	12	1.84E+04		1.87E+03	
27/04/13	11:00	22:00	11	2.07E+05		5.68E+03	

energy and one value of seismic energy per fountain were calculated by summing all energy values falling into the chosen time intervals.

If, in the case of seismic waves, scattering phenomena make the isotropic radiation assumption valid [*Kumagai et al*., 2010, 2011], the acoustic sources, as stated by *Matoza et al*. [2013], in a volcano environment are likely to be highly directional, and thus the atmosphere structure at short propagation distances poorly affects the wavefield. For these reasons, especially in case of acoustic energy, the differences between the energy values of distinct lava fountains should be taken into account rather than the absolute values. The possible presence of noise related to wind in the computation of acoustic energy is considered negligible, both because wind usually exhibits lower amplitudes with respect to the amplitude characterizing the infrasound signal during such lava fountains, and due to a visual inspection of the recorded signal, which allowed us to exclude high weather-related noise.

The lava fountain episodes taking place during February–March 2013 exhibit seismic and infrasonic energies of the order of 10^4 and 10^3 MJ, respectively. During April 2013, an evident increase of the released energies took place (Figure 4). Indeed, except for the lava fountain that occurred on 20 April, the seismic and infrasonic energies of each lava fountain had values of the order of 10^5 and 10^4 MJ, respectively. Such greater energy values relate to both higher RMS values and longer durations of the lava fountains as for instance, the 12 and 27 April episodes that showed the longest durations (more than 1 day; Figures 3a and 3b). The low energy of the 20 April episode is mainly due to the very short duration of the event (a few hours) when compared to the other lava fountains of the month (Table 1). The order of magnitude of seismic energy found in our investigations is comparable with energy values calculated with the same approach for eruptive episodes at Bezymianny volcano [*West*, 2013]. As regarding acoustic energy, at Redoubt volcano similar values were obtained for explosive eruptions lasting from few minutes to 1 h and generating plumes several kilometers higher [*McNutt et al*., 2013], while the same explosive eruptions radiated lower seismic energy (of several order of magnitude) with respect to the present results. Moreover, as expected, acoustic energy values during lava fountains are higher than those found at other volcanoes during strombolian and vulcanian explosions [*Marchetti et al*., 2009].

3.2. Gas Fluxes

The assessment of volcanic gas composition and flux is essential for the understanding and forecasting of volcanic activity, as magma degassing plays a key role in triggering and controlling the style and timing of volcanic eruptions [e.g., *Anderson*, 1975; *Oppenheimer et al*., 2003; *Williams-Jones et al*., 2008; *Edmonds*, 2008]. Daylight sulphur dioxide fluxes (SO_2 flux) from the bulk plume of Mt. Etna were measured by the FLux Automatic MEasurement (FLAME) network consisting of 10 fixed scanning ultraviolet spectrometers (Figure 1a). A complete volcanic plume-scan profile is achieved in ~5 min, and collected open-path ultraviolet spectra are reduced on site in SO_2 column densities applying the Differential Optical Absorption Spectroscopy (DOAS) methodology using a modeled reference spectrum [*Platt and Stutz*, 2008; *Salerno et al*., 2009a; *Merucci et al*., 2011]. SO_2 cross-section profiles are then transmitted to INGV-OE in Catania, where

emission rate is computed; uncertainty on SO_2 flux ranges between −22 and +36% [*Salerno et al*., 2009b; *Campion et al*., 2010; *Bonaccorso et al*., 2011].

Figure 2d shows the daily SO_2 flux between May 2012 and April 2013. Overall throughout the 1 year observation period, the emission rate was level for about 6 months before then gradually increased from late December 2012 until April 2013. In the first 5 months of 2012, the flux fluctuated widely between minimum and maximum values of 300 and 6600 tonnes per day (t/d) on 19 July and 23 May, respectively, and remained at mean values of ∼2000 t/d. The mean emission rates steadily rose to ∼2700 t/d (minimum of 600 t/d and maximum of 6000 t/d) by December, and then more sharply to 3600 t/d (minimum and maximum fluxes of 700 and 11,800 t/d) between January–April 2013. In the first 4 months of 2013, the intraday SO_2 flux showed a gradual increase between January and February 2013 peaking at ∼20,000 t/d on 22 February, and slowly dropped off in late February (Figure 3d). Between March and early April 2013, the SO_2 flux fluctuated widely with an overall declining trend. Although generally decreasing, the mean SO_2 flux was comparable with that released between January and February 2013 (∼3600 t/d) peaking at 18,500 and 20,100 t/d on 8 March and 3 April, respectively. Following the decrease recorded on 4 April, the SO_2 flux significantly rose again peaking on 27 April with 13,000 t/d.

The HCl flux was computed by combining the SO_2 flux with the SO_2/HCl ratio retrieved from open-path spectra collected by a Fourier Transform Infra-Red spectrometer (FTIR). The instrument used was a Bruker OPAG-22 (Bruker GmbH, Germany) with ZnSe beam splitter at 0.5 cm^{-1} resolution. The detector is a liquid nitrogen-cooled MCT detector with sensitivity between 1000 and 6000 cm^{-1}. The absorption spectra were collected in solar occultation mode using the Sun as the infrared source [e.g., *Francis et al*., 1998], and from different sites around the volcano (∼14 km distance from the Mt. Etna summit), depending on the volcanic plume direction and Sun position. Volcanic gas amounts were retrieved for each spectrum using a custom-made nonlinear least squares fitting analytic approach [*Rodgers*, 2000]; uncertainty in retrieved concentrations is of order of ∼4%. Molar ratios are determined by plotting the retrieved amounts of SO_2 against those of HCl. The gradients of the linear regression plot are thus expressed as SO_2/HCl ratios [e.g., *La Spina et al*., 2010]. Figure 2d shows the HCl flux calculated between May 2012 and April 2013. Between May and August 2012, the HCl flux showed a decreasing from maximum values of ∼1500 to ∼380 t/d. In the following months until December 2012, the flux was characterized by a fairly stable trend around values of ∼500 t/d. In late December 2012, the flux began to increase peaking in February 2013 with values of ∼2000 t/d (Figure 3d).

3.3. Radiometry

The study of heat fluxes and temperature variations at active volcanoes provides a key contribution to understanding of volcanic processes, and to volcanic hazard assessment and risk management [e.g., *Spampinato et al*., 2011]. The integration of thermal data with geophysical and geochemical signals, has provided useful insights of eruption onsets and eruptive dynamics [e.g., *Chrétien and Brousse*, 1989; *Connor et al*., 1993; *Flynn et al*., 1993; *Oppenheimer et al*., 1993a; *Dehn et al*., 2002; *Dean et al*., 2004; *Burgi et al*., 2002; *Branan et al*., 2008; *Spampinato et al*., 2013]. For this study, thermal investigations were carried out by using a permanent radiometer integrated in the EBEL seismic station (Figures 1a and 1b) [*Murè et al*., 2013]. The instrument consisted of an Optris CT LT15F infrared thermometer sensitive in the 8–14 μm waveband and with system accuracy of ±1% at ambient temperature of 23±5° C, optical resolution of 15:1 (90% radiation energy), and response time of 9 ms in analog output. The detector can record thermal signals according to dynamic ranges between −50 and 975°C and at sampling rate of 50 Hz. For EBEL's radiometer recording, we used emissivity of 0.97, transmissivity of 0.85 (in agreement with the absorption effect of the external protective lens used), and a dynamic range of −20 to 950°C (to avoid signal saturation). External temperature reference was automatically and simultaneously acquired by the instrument. Considering the mean line-of-sight of 1 km (radiometer to crater rim), the radiometer field-of-view (FOV) consisted of a circular area of ∼3490 m^2 (Figure 1 b) including a small portion of the very top part of NSEC rim but with most of the part being clear sky (in the absence of fumarolic/eruptive activity). For this study, we considered the RMS of the 50 Hz signal calculated over a time window of 1 min (Figure 2e). Note that apparent temperatures are underestimated with respect to absolute values due to the broad radiometer FOV, the mixed nature of the different temperature components falling within it, and factors affecting remote thermal measurements [e.g., *Spampinato et al*., 2011]. However, we are not actually interested in absolute temperature retrieval but rather in variations of the signal indicative of eruptive activity [e.g., *Harris et al*., 2003].

For this study, we considered data continuously acquired from 1 May 2012 until 28 February 2013 (Figure 2e), when the EBEL station was buried by the NSEC lava flows. Between 1 May and 8 August 2012, the radiometer did not record any significant temperature variations related to eruptive activity, but only the increasing pattern of the diurnal-nocturnal oscillations due mainly to the crater area solar heating and cooling (Figure 2e) [e.g., *Spampinato et al*., 2011]. On 9 August 2012, the temperature signal peaked suddenly at ~150°C, thus marking the passage of BN crater's products within the radiometer FOV (Figures 1c and 2e). The lack of radiometric information at the start of the BN eruption on 3 July 2012 relates to distance from the target and the fact that the activity was confined within the BN crater. The combined factors significantly attenuated the amplitude of the radiometric signal, resulting in a low volcanic-associated signal covered by the higher amplitude diurnal-nocturnal temperature variations. From September to December 2012, no significant changes associated with eruptive activity were reported.

In January 2013, apparent temperatures fluctuated between 0 and 12°C (mean of 3.5°C, standard deviation of 2.0) accordingly with weather conditions and to the sporadic fumarolic activity from NSEC summit and the background BN and VOR volcanic plume. Similarly, the overall trend of early February 2013 showed quite low temperature values punctuated by minor peaks below ~10°C (Figures 2e and 3e) associated with either gas emissions from the crater summit entering the radiometer FOV and/or increased fumarolic activity from the NSEC rim and BN and VOR activity. At ~01:00 (all times are in GMT) of 19 February 2013, temperature went to 0°C before the rapid increase that started ~2 and half hours later, leading to the first 2013 paroxysm from NSEC (Figures 2e and 3e). Temperature peaked at 04:10 passing in ~1 h from 0 to ~430°C, time interval during which the eruptive regime observed at the surface changed from pure strombolian and lava outpouring to lava fountain activity through a rapid transitional phase (Figures 2e and 3e) [e.g., *Parfitt*, 2004; *Spampinato et al*., 2008].

Following the first paroxysm, five other events caused temperature signals to peak at maximum values of 77 and 100°C on 20 February 2013 at 01:09 and 13:35, respectively, 70°C on 21 February 2013 at 04:47, 165°C on 23 February 2013 at 18:41, and 100°C on 28 February 2013 at 10:11 (Figures 2e and 3e). Overall, the paroxysmal events displayed the typical waveform of rapid heating of the targeted area and successive gradual cooling to low temperature values [e.g., *Harris et al*., 2003, 2005; *Sahetapy-Engel et al*., 2008]. In all cases, given the FOV geometry, the heating phase consisted of the superposition of two sources: heat released by ballistics during the discrete explosive activity and lava fountain jetting, and heat released by the hot pyroclasts accumulating on the crater rim portion falling in the radiometer FOV (Figure 1b).

3.4. GPS Data

In the last decade, GPS technique has become one of the most commonly used methodology for continuous monitoring of volcano deformation (e.g., at Kilauea, Hawaii [*Montgomery-Brown et al*., 2011]; at Mount St. Helens, Washington [*Lisowski et al*., 2008]; at Piton de La Fournaise, La Réunion [*Peltier et al*., 2010]). GPS technique is able to capture, with high resolution, any changes of the volcano shape, and when combined with appropriate source models, provides key constraints on subsurface magma storages and conduits [e.g., *González and Palano*, 2014].

The GPS permanent network of Mt. Etna consists of 39 stations, equipped with receivers (models GMX902, GRX1200, SR530) and antenna (models LEIAT504, LEIAX1202, LEIAR10) manufactured by Leica Geosystems (Figure 1c). Daily GPS time series and geodetic velocities were reduced using the GAMIT/GLOBK software [*Herring et al*., 2010] and following the method described in *González and Palano* [2014]. A local reference frame—Etn@ref—was considered in the computation to isolate the volcanic deformation from the background tectonic pattern [*Palano et al*., 2010]. In order to detect significant changes associated with Mt. Etna activity, temporal records of areal variation of two triangles sited at the volcano summit (~2800 m a.s.l.) and intermediate altitude (~1500 m a.s.l.) were retrieved (Figure 1c) [e.g., *Aloisi et al*., 2011]. The summit triangle relates to the ECNE-EINT-ECPN stations and is able to track the movement of magma within the shallower portion of the volcano plumbing system, while the intermediate-altitude triangle refers to EMGL-ESLN-EMSG stations, and provides insights into magma movement in a deeper portion of the plumbing system.

Results revealed two main ground deformation stages (expressed in ppm, Figure 2f). Both time series show positive areal deformation from May 2012 to mid-February 2013 followed by a prevailing negative areal change, which lasts until April 2013. During the NSEC lava fountain sequence, the negative areal pattern follows a quasi-linear trend for the intermediate triangle, whereas the summit one displays a small positive

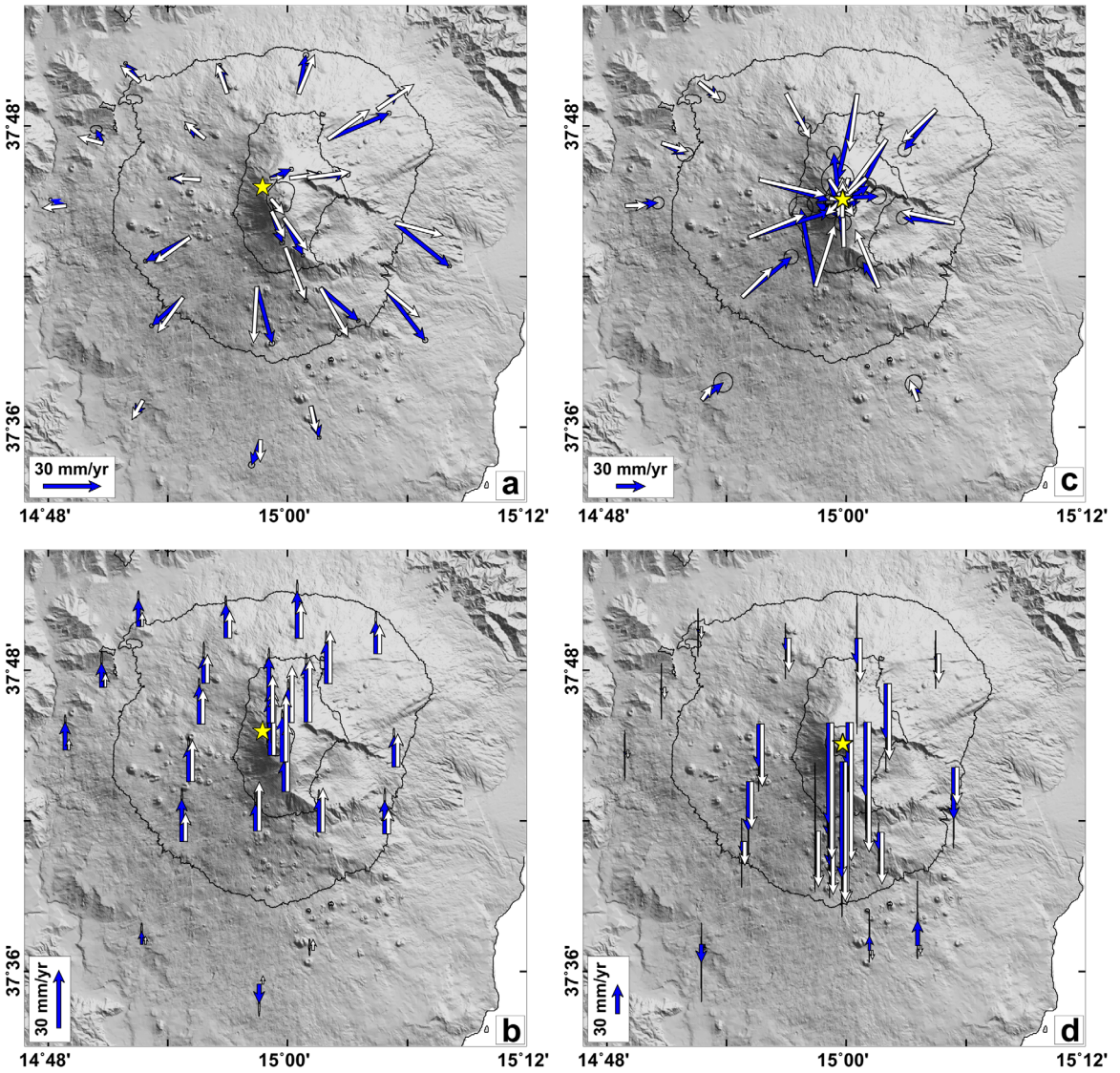

Figure 5. Comparison between observed (blue arrows) and modeled (white arrows) (a and c) horizontal and (b and d) vertical geodetic velocities relevant to the considered time intervals: (a, b) for 1 May 2012 to 18 February 2013 and (c, d) for 19 February 2013 to 30 April 2013. Locations of modeled sources are reported as yellow stars.

areal change between 27 February and 1 April 2013 (Figure 3f). The different pattern of the two records suggests different responses of the shallow and deep portions of the plumbing systems. As no consistent deformation pattern is discernible from 27 February to 1 April in the intermediate triangle area—i.e., (i) the deformation seems to affect only the stations located near the summit area and (ii) the associated uncertainties are of the same magnitude as the signals—we calculated the ground deformation pattern for the whole NSEC lava fountain sequence period. The estimated surface ground velocity field for the pre and syn-lava fountaining periods are reported in Figure 5.

From May 2012 to mid-February 2013, the ground deformation field (Figures 5a and 5b) is characterized by a general radial pattern of surface displacement of the volcano with uplift of ~35 mm/yr centered westward of the summit area, and clearly depicting a general inflation of the volcano edifice. Conversely, the NSEC lava fountain sequence period is characterized by a volcano-wide deflation with negative height variations up to 120 mm/yr close to the summit area (Figures 5c and 5d).

Both ground velocity fields were used as input to constrain isotropic half-space elastic inversion models. Values of 30 GPa and 0.25 were assumed for the shear modulus and Poisson's ratio in the half-space,

Table 2. Estimated Parameters and Associated Uncertainties for the Two Ground Deformation Sources Modeled for the P1 and P2 Periods[a]

	Yang Magmatic Pressure Source (See *Yang et al.* [1988] for Parameter Descriptions) for P1	*Mogi* Magmatic Pressure Source (See *Mogi* [1958] for Parameter Descriptions) for P2
East UTM (m)	498195 ± 35	499739 ± 101
North UTM (m)	4179116 ± 43	4178246 ± 143
Depth (m a.s.l.)	−6511 ± 167	−5493 ± 381
ΔVolume (m^3)	11.1 ± 1.2 ·10^6	6.0 ± 1.1 ·10^6
Major Axis (m)	110 ± 88 m	
Axes Ratio	0.27 ± 0.05	
Strike (°)	49 ± 2	
Plunge (°)	108 ± 0.5	

[a]Coordinates are in UTM 33N projection.

respectively; the chosen rigidity represents an average value for Mt. Etna crust [*Chiarabba et al.*, 2000] and corresponds to the values commonly used for Mt. Etna modeling [e.g., *Palano et al.*, 2008; *Bonanno et al.*, 2011]. Following the criterion described in *Cannavó* [2012], we adopted the *Yang et al.* [1988] and the *Mogi* [1958] analytical pressure sources to model the observed ground velocity pattern for inflation and deflation periods (i.e., pre and syn-lava fountaining periods), respectively. Inversions were performed using a combination of genetic algorithms [*Tiampo et al.*, 2000] and nonlinear least squares approaches [*Morè*, 1977]. To account for the effects of topography, we included in the computation, the method of *Williams and Wadge* [2000]. In the computation, both horizontal and vertical GPS components were inverted taking into account weights proportional to the associated displacement errors. Estimation of the uncertainties in best-fitting parameters was performed by adopting the Jackknife sampling method [*Efron*, 1982]. For each considered time interval, the estimated parameters of the source are shown in Table 2. For the May 2012 to mid-February 2013 period, the best model is given by a near vertical elongated ellipsoidal source centered at ∼ −6500 m (a.s.l.) beneath the upper western flank of the volcano (Figures 5a and 5b; Table 2) and characterized by a positive volume change of $\sim 11 \times 10^6$ m^3. For the lava fountain sequence period, the best model is given by a spherical source centered at ∼−5500 m (a.s.l.) beneath the summit area (Figures 5c and 5d; Table 2) and characterized by a negative volume change of $\sim 6 \times 10^6$ m^3.

4. Data Interpretation and Discussion

Integration of the geophysical, infrared, and geochemical data allowed us to characterize the volcanic activity in the first months of 2013 at monthly and daily scales; as well as to assess the significance of the NSEC paroxysms in the eruptive framework of Mt. Etna at least since May 2012. While, the seismic, infrasound and radiometric signals provided description of each of the 13 paroxysmal events, the SO_2 and HCl fluxes helped assess the likely mechanisms on the basis of the February–April 2013 paroxysmal activity at NSEC, and GPS data provided constraints on magma movement at depth within the volcano plumbing system. Figure 2 shows the trend of variability of seismic and infrasonic RMS, SO_2 and HCl fluxes, apparent temperature, and ground deformation between May 2012 and April 2013. In the following paragraphs we discuss the 1 year time window by discriminating two periods: Period P1 and Period P2. P1 spans from 1 May 2012 to 18 February 2013 and P2 includes the period between 19 February and 30 April 2013 (Figure 2).

4.1. Period P1

Overall in period P1, neither the seismic and acoustic signals nor the radiometric measurements detected any significant variation associated with the NSEC activity (Figure 2). The only exceptions were the weak infrasonic events detected from 21 November 2012 (when crater incandescence occurred) to at least 27 November 2012, which led to a slight increase in the infrasonic RMS. During P1 the most relevant signals ascribable to eruptive activity were those produced by BN crater starting in July 2012 [*INGV-OE Internal Report*, 2012h]. BN activity irregularly lasted until August, and successively occurred on 2 and 18 October [*INGV-OE Internal Report*, 2012i, 2012j] (Figures 2a and 2b). Thermal radiation produced by the strombolian explosions and the emplacing lava flows was recorded by the EBEL radiometer with peaks between ∼40 and 150°C (Figure 2e). From May to August 2012, SO_2 and HCl fluxes showed fluctuating steady trends suggesting that although the BN July–August eruptive activity was occurring, no any new volatile-rich magma was supplied to the shallow volcano feeding system (∼−1000 to −2000 m a.s.l.) [*Spilliaert et al.*, 2006] (Figure 2d). Accordingly, the eruptive activity at the two craters might have been fed by magma already resident in the volcano upper conduit and likely by the same batch of magma that supplied the previous 2012

eruptive activity [*Behncke et al*., 2014]. This scenario agrees well with the predominance of HCl flux released from May to September 2012 with respect to SO_2. The prevalence of HCl flux is indicative, in fact, of residual degassing of a batch of magma relatively depleted in volatile content, at shallow depths (HCl exsolution depths at ∼1000–2000 m a.s.l.) [e.g., *Oppenheimer et al*., 2014]. The only evidence of changes in the volcano plumbing system was related to the linear positive trend of the surface areal time series calculated by GPS data (Figure 2f) produced by a −6500 m a.s.l. deep pressurizing source located under the volcano's upper-western flank [e.g., *Dvorak and Dzurisin*, 1993] (Figures 5a and 5b; Table 2). In September 2012, the SO_2 emission rates started increasing while HCl fluxes continued showing the same stable trend of the previous months. HCl started increasing in October, although the two fluxes showed decoupling trends that became significant in December 2012, with the SO_2 flux dominating over the HCl flux. Such behavior, coupled with the geodetic data (Figures 5a and 5b; Table 2), suggests refilling of the volcano feeding system by volatile-rich magma [e.g., *Dvorak and Dzurisin*, 1993].

Between 3 January and 17 February 2013, Mt. Etna's summit activity consisted in episodic strombolian intracrater activity at BN, and occasionally at VOR, as well as intense degassing to strombolian activity at NSEC (P1 in Figure 2) [e.g., *INGV-OE Internal Report*, 2013a, 2013b, 2013c, 2013d, 2013e, 2013f]. The eruptive activity at the three summit craters produced low amplitude infrasound transients, not detectable in the RMS, and peaking of the radiometric signal, though, due to the distance from the detector, the amplitude of the BN and VOR transients resulting were significantly attenuated. The SO_2 and HCl fluxes positively correlated in January showing gradual and continuous increasing trends, and anticorrelated in the first half of February, prior to the start of the NSEC paroxysmal activity (Figure 2d). At open-vent volcanoes, decouplings among gas species have been commonly associated with inefficient degassing dynamics, and thus with pressurization of the volcanic plumbing systems [e.g., *Aiuppa et al*., 2011].

4.2. Period P2

Period P2, whose magnification is provided in Figure 3, displayed intense and impulsive eruptive activity from NSEC with episodes of lava fountaining, surprisingly closely spaced in time in the early days. Of this period of paroxysmal activity, we analyze only radiometric data of the first five paroxysms and the start of the sixth, which does not allow for statistical investigations. NSEC activity was characterized by deflation due to the depressurization of a source located at ∼ −5500 m (a.s.l.) beneath the summit area (Figures 5c and 5d).

Characterization of each lava fountain episode by detailed analysis of the seismic and acoustic signals revealed an increase of the released cumulated energy trends over time according to two distinguished trends—i.e., the February–early April 2013 and April 2013 curves (Figure 4). Focusing on the February–early April period, the relationships of seismic and acoustic energy versus time indicates that the paroxysmal episodes progressively became more energetic and less close in time. As already observed by *La Spina et al*. [2015] and based on this evidence, we suggest that the longer the interevent time, and thus the time needed for the NSEC feeding system to reach the threshold pressure to trigger the subsequent lava fountain, the greater the energy accumulated and then released. Figure 6 details the relation between interevent time (i.e., interevent time between the start of a fountain episode and the start of the previous one) and time of occurrence. The graph exhibits a linear increase of the interevent time with elapsed time from the first episode to the 3 April lava fountain and scattered behavior for the remaining paroxysms. Combining Figures 4 and 6, we note that a clear change of both the trend of cumulative seismic and acoustic energy and the interevent time took place after the 3 April episode. This paroxysm seems to discriminate between two sequences of lava fountains showing slightly different seismological behaviors. In fact, although the paroxysms following the 3 April episode also show a linear relation between the cumulative curves and time, the slope of the curve increases (Figure 4) and the linear relation of the interevent time observed in February–March is no longer visible (Figure 6). These changes in the eruptive behavior might be partially explained considering a gradual increase in the efficiency of magma transport and degassing as soon as the upper feeding system stabilizes, and an increase in the rate of accumulation of energy.

The benchmark role of the 3 April 2013 lava fountain pinpoints two eruptive phases in P2. Indeed, this event showed slightly more evolved magma composition with respect to those observed in the previous February–March lava fountains that *Corsaro and Miraglia* [2013a] attributed to processes of magma cooling and crystallization. These processes are consistent with the interevent times between the 16 March and 3 April

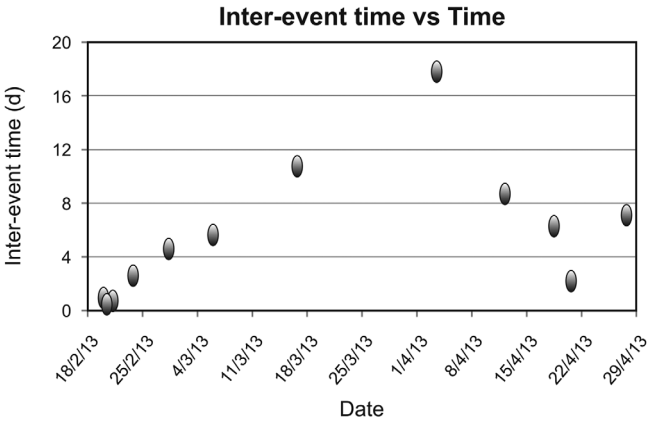

Figure 6. Time intervals (days) between a lava fountain and the previous one (called interevent time) plotted versus the lava fountain occurrence time.

paroxysms, which are greater than those observed between the other episodes, and with the geochemical signals. The declining trends of both SO_2 and HCl fluxes displayed until the end of March (Figure 3d) suggest depletion of the volatile content in the shallow supply system. In this view, the paroxysms of the February–3 April time window seem to fall within an overall degassing cycle that started as early as October 2012, and with the majority of magmatic volatiles released between February and March 2013 (Figure 2d). The decoupling behavior of the SO_2 and HCl fluxes recorded since October 2012 reflects gradual conduit-filling by a volatile-rich batch of magma in the volcano shallow feeding system. The increasing degassing mode sped up in December 2012 prior to climaxing in the second half of February and driving the renewal of the paroxysmal activity at NSEC; the gas input eventually lasted until early April 2013. Since March, the gradual decline of both SO_2 and HCl fluxes, combined with their recoupling, indicated degassing of a residual volatile poor batch of magma residing in the shallow volcano feeding system.

After the 3 April episode, an additional four paroxysms occurred on 12, 18, 20, and 27 April. The paroxysms exhibited higher seismic and acoustic energy with respect to those of the February–3 April phase, except for the 20 April episode, which was less energetic compared to the other events (Figure 4). Petrology evidence suggests slightly less evolved magma compositions during the paroxysms of 12, 18, and 20 April [*Corsaro and Miraglia*, 2013b], and more evolved in that of the 27 April lava fountain [*Corsaro and Miraglia*, 2013c]. The integration of seismic and petrological observations might indicate that after the 3 April paroxysm, a volatile-rich batch of magma reinjected into the NSEC supply system; however this hypothesis is in contrast with the SO_2 and HCl flux rates (Figures 2d and 3d). In facts the trends of both gas emission rates showed an overall decrease marked by fluctuations associated with each of the April lava fountains (Figure 3d). The geochemical evidence is consistent with the areal changes of the intermediate-altitude deformation triangle which does not show any variation (Figures 2f and 3f). The slight inflation recorded for the week preceding the 3 April lava fountain, whose geodetic signals are of same magnitude as the associated uncertainties, is in the fact that it is observed only at the stations close to the summit area (Figures 2f and 3f), suggesting the presence of a very shallow pressurizing magmatic reservoir. In this view, we propose that no new volatile-rich batch of magma entered the NSEC feeding system, but rather that the same February–March batch was still involved with the less evolved products erupted in April, likely representing its deeper portion. In this light, the small inflation of the shallow magma reservoir might have been triggered by magma rising to the surface, which promoted volatile exsolution and boiling. The occurrence of the post 3 April lava fountains might have been caused by self-induced formation of bubbles that allowed buildup of pressure within the shallow feeding system prior to each of the post-3 April episodes [*Tait et al*., 1989; *Métrich et al*., 1993; *La Delfa et al*., 2001; *Corsaro and Pompilio*, 2004; *Vergniolle and Gaudemer*, 2012]. The increasing overpressure inside the very shallow portion of the plumbing system (>2000 m a.s.l.) [*Cannata et al*., 2013], at the same time as the onset of the lava fountain cycle, was also observable in the LP signals. LP events, in fact, increased in both number and amplitude at the end of February 2013. A further observation from comparison of interevent times versus seismic energies of the 9 of the 13 episodes recorded by the EMFO station (Figure 7), is that the lava fountains with interevent times shorter than 6 days were characterized by seismic energies lower than 5×10^4 MJ, while the lava fountains with longer interevent times (except for the 16 March episode) characterized by energies higher than 5×10^4 MJ (Figure 7).

As with the lava fountains of the first phase, this behavior can be interpreted as follows: the longer the interevent time between events, and thus time needed for the NSEC feeding system to reach the threshold pressure to trigger a lava fountain, the greater the energy accumulated and then released.

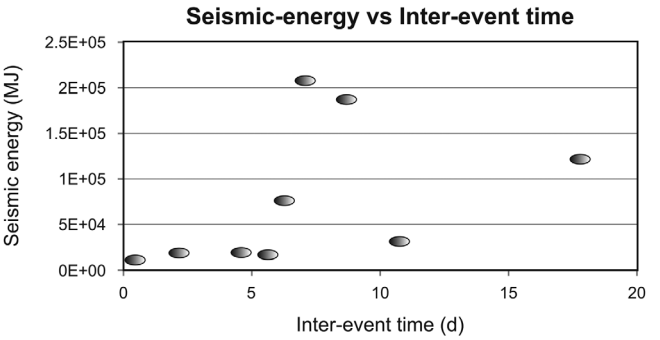

Figure 7. Seismic energies (MJ) of lava fountains plotted versus their interevent times (days).

5. Concluding Remarks

The integration of geophysical, geochemical, and radiometric observations enabled detailed study of Mt. Etna's NSEC eruptive activity between February and April 2013 and the related preeruptive conditions of the volcano plumbing system since May 2012. The main considerations that arose from this multiparametric investigation are the following:

1. The eruptive activity of the BN crater recorded in July–August 2012 was fed by the same magma that supplied the previous 2012 NSEC lava fountain cycle. The first signals of the volcano feeding system recharge were recorded initially by ground deformation data, and then by geochemical data starting from May and October 2012, respectively;
2. The relationships of seismic and acoustic energy versus time suggests that the paroxysmal episodes progressively became more energetic and less close in time;
3. The February–April 2013 lava fountain cycle is accompanied by a volcano-wide deflation due to depressurization of a source located at ∼−5500 m (a.s.l.) beneath the summit area;
4. This cycle is divided into two parts by the 3 April 2013 episode, which showed geophysical and petrological differences with respect to the previous February–March paroxysms. Based on our observations, we propose that the differences between the February–March and April lava fountains might be partly explained by increase in the efficiency of the magma transport and degassing associated with stabilization of the upper feeding system;
5. Geochemical data suggest that the paroxysms of the February–3 April fall within an overall degassing cycle that started as early as October 2012 and with the majority of magmatic volatiles released between February and March 2013. In this view, as also suggested by ground deformation data and LP events, no reinjection of the shallow feeding system occurred afterward, and thus the following April 2013 paroxysms may result from self-induced formation of bubbles that allowed buildup of pressure within the shallow feeding system prior to each of the episodes.

Overall, our study has contributed to the understanding of Mt. Etna's eruptive behavior that, since January 2011, has changed its regime from prevalently effusive to more violent, almost cyclic explosive characteristics. Indeed this is not novel to Mt. Etna's eruptive activity history; however, what has changed is the opportunity to track such variations by multidisciplinary, quantitative means. Future investigations might focus on modeling of the eruptive events at multiple scales and on identification of the likely factors on the basis of such modifications in the volcano eruptive regime.

Acknowledgments
The authors kindly acknowledge, G. Larocca, L. Scuderi, P. Montalto, F. Ferrari, F. Murè for their technical support and suggestions. S. Di Prima is thanked for his availability in scheduling the technical surveys to EBEL station. L. Spampinato and T. Caltabiano are grateful to S. Consoli and O. Consoli for their logistic support for reaching EBEL station in winter period. D. Pellegrino, M. Pulvirenti and M. Rossi are kindly acknowledged for managing the permanent GPS network and providing raw data. L. Spampinato is indebted with S. Giammanco and G. Puglisi for having supported her research activity by the VIGOR (Valutazione del potenzlale Geotermico delle RegiOni della conveRgenza) and the European FP7 MED-SUV (MEditerranean SUpersite Volcanoes, grant agreement 308665) projects. A. La Spina received funding from the European Research Council under the European FP7 (FP/2007–2013)/ERC grant agreement 279802 through the CO_2Volc project. M. Sciotto research was funded by SIGMA (Sistema Integrato di sensori in ambiente cloud per la Gestione Multirischio Avanzata) project (PON01_00683). Data used for this study belong to INGV. The authors thank the INGV-OE personnel that produced the INGV Internal Reports here cited. The authors thank Glyn Williams-Jones and an anonymous reviewer for their detailed comments and fruitful suggestions.

References

Acocella, V., and M. Neri (2003), What makes flank eruptions? The 2001 Etna eruption and its possible triggering mechanisms, *Bull. Volcanol.*, *65*, 517–529.

Aiuppa A., M. Burton, P. Allard, T. Caltabiano, G. Giudice, S. Gurrieri, M. Liuzzo, and G. Salerno (2011), First experimental evidence for the CO_2-driven origin of Stromboli's major explosions, *Solid Earth Discuss.*, *3*, 411–430, doi:10.5194/sed-3-411-2011.

Allard, P., M. Burton, and F. Murè (2005), Spectroscopic evidence for a lava fountain driven by previously accumulated magmatic gas, *Nature*, *433*, 407–410.

Aloisi, M., M. Mattia, C. Ferlito, M. Palano, V. Bruno, and F. Cannavò (2011), Imaging the multi-level magma reservoir at Mt. Etna volcano (Italy), *Geophys. Res. Lett.*, *38*, L16306, doi:10.1029/2011GL048488.

Alparone, S., D. Andronico, L. Lodato, and T. Sgroi (2003), Relationship between tremor and volcanic activity during the Southeast Crater eruption on Mount Etna in early 2000, *J. Geophys. Res.*, *108*(B5), 2241, doi:10.1029/2002JB001866.

Anderson, A.T. (1975), Some basaltic and andesitic gases, *Rev. Geophys.*, *13*(1), 37–55.

Andronico, D., and R. A. Corsaro (2011), Lava fountains during the episodic eruption of South-East Crater (Mt. Etna), 2000. Insights into magma-gas dynamics within the shallow volcano plumbing system, *Bull. Volcanol.*, *73*, 1165–1178.

Andronico, D., et al. (2005), A multi-disciplinary study of the 2002-03 Etna eruption: Insights into a complex plumbing system, *Bull. Volcanol.*, *67*, 314–330.

Andronico, D., M. D. Lo Castro, M. Sciotto, and L. Spina (2013), The 2010 ash emissions at the summit craters of Mt Etna: Relationship with seismo-acoustic signals, *J. Geophys. Res. Solid Earth*, *1*, 51–70, doi:10.1029/2012JB009895.

Behncke, B., M. Neri, E. Pecora, and V. Zanon (2006), The exceptional activity and growth of the Southeast Crater, Mount Etna (Italy), between 1996 and 2001, *Bull. Volcanol.*, *69*(2), 149–173, doi:10.1007/s00445-006-0061-x.

Behncke, B., S. Branca, R. A. Corsaro, E. De Beni, L. Miraglia, and C. Proietti (2014), The 2011–2012 summit activity of Mount Etna: Birth, growth and products of the new SE crater, *J. Volcanol. Geotherm. Res.*, *270*, 10–21.

Bonaccorso, A., et al. (2011), Dynamics of a lava fountain revealed by geophysical, geochemical and thermal satellite measurements: The case of the 10 April 2011 Mt Etna eruption, *Geophys. Res. Lett.*, *38*, L24307, doi:10.1029/2011GL049637.

Bonaccorso, A., S. Calvari, G. Currenti, C. Del Negro, G. Ganci, A. Linde, R. Napoli, S. Sacks, and A. Sicali (2013), From source to surface: Dynamics of Etna's lava fountains investigated by continuous strain, magnetic, ground and satellite thermal data, *Bull. Volcanol.*, *75*, 690, doi:10.1007/s00445-013-0690-9.

Bonaccorso, A., S. Calvari, A. Linde, and S. Sacks (2014), Eruptive processes leading to the most explosive lava fountain at Etna volcano: The 23 November 2013 episode, *Geophys. Res. Lett.*, *41*, 4912–4919, doi:10.1002/2014GL060623.

Bonanno, A., M. Palano, E. Privitera, S. Gresta, and G. Puglisi (2011), Magma intrusion mechanisms and redistribution of seismogenic stress at Mt. Etna volcano (1997–1998), *Terra Nova*, *23*, 339–348, doi:10.1111/j.1365-3121.2011.01019.x.

Branan Y. K., A. Harris, I. M. Watson, J. C. Phillips, K. Horton, G. Williams-Jones, and H. Garbeil (2008), Investigation of at-vent dynamics and dilution using thermal infrared radiometers at Masaya volcano, Nicaragua, *J. Volcanol. Geotherm. Res.*, *169*, 34–47.

Branca, S., and P. Del Carlo (2005), Types of eruptions of Etna volcano AD 1670–2003: Implications for short-term eruptive behavior, *Bull. Volcanol.*, *67*, 732–742.

Burgi, P. Y., M. Caillet, and S. Haefeli (2002), Field temperature measurements at Erta 'Ale Lava Lake, Ethiopia, *Bull. Volcanol.*, *64*, 472–485.

Burton, M. R., et al. (2005), Etna 2004–2005: An archetype for geodynamically-controlled effusive eruptions, *Geophys. Res. Lett.*, *32*, L09303, doi:10.1029/2005GL022527.

Calvari, S., G. G. Salerno, L. Spampinato, M. Gouhier, A. La Spina, E. Pecora, A. J. L. Harris, P. Labazuy, E. Biale, and E. Boschi (2011), An unloading foam model to constrain Etna's 11–13 January 2011 lava fountaining episode, *J. Geophys. Res.*, *116*, B11207, doi:10.1029/2011JB008407.

Campion, R., G. G. Salerno, P.-F. Coheur, D. Hurtmans, L. Clarisse, K. Kazahaya, M. Burton, T. Caltabiano, C. Clerbaux, and A. Bernard (2010), Measuring volcanic degassing of SO_2 in the lower troposphere with ASTER band ratios, *J. Volcanol. Geotherm. Res.*, *194*(1-3), 42–54.

Cannata, A., M. Hellweg, G. Di Grazia, S. Ford, S. Alparone, S. Gresta, P. Montalto, and D. Patanè (2009a), Long period and very long period events at Mt. Etna volcano: Characteristics, variability and causality, and implications for their sources, *J. Volcanol. Geotherm. Res.*, *187*, 227–249, doi:10.1016/j.jvolgeores.2009.09.007.

Cannata, A., P. Montalto, E. Privitera, G. Russo, and S. Gresta (2009b), Tracking eruptive phenomena by infrasound: May 13, 2008 eruption at Mt. Etna, *Geophys. Res. Lett.*, *36*, L05304, doi:10.1029/2008GL036738.

Cannata, A., G. Di Grazia, M. Aliotta, C. Cassisi, P. Montalto, and D. Patané (2013), Monitoring seismo-volcanic and infrasonic signals at volcanoes: Mt. Etna case study, *Pure Appl. Geophys.*, *170*, 1751–1771.

Cannavó, F. (2012), Sensitivity analysis for volcanic source modeling quality assessment and model selection, *Comput. Geosci.*, *44*, 52–59, doi:10.1016/j.cageo.2012.03.008.

Caplan-Auerbach, J., A. Bellesiles, and J. K. Fernandes (2010), Estimates of eruption velocity and plume height from infrasonic recordings of the 2006 eruption of Augustine Volcano, Alaska, *J. Volcanol. Geotherm. Res.*, *189*, 12–18, doi:10.1016/j.jvolgeores.2009.10.002.

Chiarabba, C., A. Amato, E. Boschi, and F. Barberi (2000), Recent seismicity and tomographic modeling of the Mount Etna plumbing system, *J. Geophys. Res.*, *105*(B5), 10,923–10,938, doi:10.1029/1999JB900427.

Chouet, B. (1996), Long-period volcano seismicity: Its source and use in eruption forecasting, *Nature*, *380*, 309–316.

Chrétien, S., and R. Brousse (1989), Events preceeding the great eruption of 8 May, 1902 at Mount Pelée, Martinique, *J. Volcanol. Geotherm. Res.*, *38*, 67–75.

Connor, C. B., B. M. Clement, S. Xiaodan, S. B. Lane, and J. West-Thomas (1993), Continuous monitoring of high-temperature fumaroles on an active lava dome, Volcan Colima, Mexico: Evidences of mass flow variation in response to atmospheric forcing, *J. Geophys. Res.*, *98*(B11), 19,713–19,722.

Corsaro, R. A., and L. Miraglia (2013a), Composizione dei vetri dei prodotti emessi dal Nuovo Cratere di Sud-Est durante la fontana di lava del 3 aprile 2013, *Rapp. UFVG del 11/04/2013*, Catania, Italy. [Available at www.ct.ingv.it.]

Corsaro, R. A., and L. Miraglia (2013b), Composizione dei vetri dei prodotti emessi dal Nuovo Cratere di Sud-Est durante la fontana di lava del 12 aprile 2013, *Rapp. UFVG del 16/04/2013*, Catania, Italy. [Available at www.ct.ingv.it.]

Corsaro, R. A., and L. Miraglia (2013c), Composizione dei vetri dei prodotti emessi dal Nuovo Cratere di Sud-Est durante le fontane di lava del 20 e 27 aprile 2013, *Rapp. UFVG del 17/05/2013*, Catania, Italy. [Available at www.ct.ingv.it.]

Corsaro, R. A., and M. Pompilio (2004), Magma dynamics in the shallow plumbing system of Mt. Etna as recorded by compositional variations in volcanics of recent summit activity (1995–1999), *J. Volcanol. Geotherm. Res.*, *137*, 55–71.

Dabrowa, A. L., D. N. Green, A. C. Rust, and J. C. Phillips (2011), A global study of volcanic infrasound characteristics and the potential for long-range monitoring, *Earth Planet. Sci. Lett.*, *310*, 369–379, doi:10.1016/j.epsl.2011.08.027.

Dean, K. G., J. Dehn, K. R. Papp, S. Smith, P. Izbekov, R. Peterson, C. Kearney, and A. Steffke (2004), Integrated satellite observations of the 2001 eruption of Mt. Cleveland, Alaska, *J. Volcanol. Geotherm. Res.*, *135*, 51–73.

Dehn, J., K. G. Dean, K. Engle, and P. Izbekov (2002), Thermal precursors in satellite imagery of the 1999 eruption of Shishaldin Volcano, *Bull. Volcanol.*, *64*, 525–534.

Dvorak, J. J., and D. Dzurisin (1993), Variations in magma supply rate at Kilauea volcano, Hawaii, *J. Geophys. Res.*, *98*(2), 22,255–22,268.

Edmonds, M. (2008), New geochemical insights into volcanic degassing, *Philos. Trans. R. Soc. A*, *366*, 4559–4579, doi:10.1098/rsta.2008.0185.

Efron, B. (1982), *The Jackknife, the Bootstrap and Other Resampling Plans*, vol. 38, pp. 1–92, Soc. for Ind. and Appl. Math., Philadelphia, Pa., doi:10.1137/1.9781611970319.

Endo, K., T. Chiba, H. Taniguchi, M. Sumita, S. Tachikawa, T. Miyahara, R. Uno, and N. Miyaji (1988), Tephrochronological study on the 1986–1987 eruptions of Izu-Oshima volcano, Japan, *Bull. Volcanol. Soc. Jpn.*, *33*, S32–S51.

Fee, D., M. Garces, and A. Steffke (2010), Infrasound from Tungurahua Volcano 2006–2008: Strombolian to Plinian eruptive activity, *J. Volcanol. Geotherm. Res.*, *193*, 67–81, doi:10.1016/j.jvolgeores.2010.03.006.

Flynn, L. P., P. J. Mouginis-Mark, J. C. Gradie, and P. G. Lucey (1993), Radiative temperature measurements at Kupaianaha lava lake, Kilauea volcano, Hawaii, *J. Geophys. Res.*, *98*(B4), 6461–6476.

Francis, P., M. R. Burton, and C. Oppenheimer (1998), Remote measurement of volcanic gas compositions by solar occultation spectroscopy, *Nature*, *396*, 567–570.
Friedman, P. D., W. J. Meyer, and S. Carey (2006), Experimental simulation of phase mingling in a subaqueous lava fountain, *J. Geophys. Res.*, *111*, B07201, doi:10.1029/2005JB004162.
Ganci, G., A. J. L. Harris, C. Del Negro, Y. Guehenneux, A. Cappello, P. Labazuy, S. Calvari, and M. Gouhier (2012), A year of lava fountaining at Etna: Volumes from SEVIRI, *Geophys. Res. Lett.*, *39*, L06305, doi:10.1029/2012GL051026.
González, P. J., and M. Palano (2014), Mt. Etna 2001 eruption: New insights into the magmatic feeding system and the mechanical response of the western flank from a detailed geodetic dataset, *J. Volcanol. Geotherm. Res.*, *274*, 108–121, doi:10.1016/j.jvolgeores.2014.02.001.
Gouhier, M., A. Harris, S. Calvari, P. Labazuy, Y. Guehenneux, F. Donnadieu, and S. Valade (2012), Lava discharge during Etna's January 2011 fire fountain tracked using MSG-SEVIRI, *Bull. Volcanol.*, *74*(4), 787–793, doi:10.1007/s00445-011-0572-y.
Harris, A. J. L., et al. (2003), Ground-based infrared monitoring provides new toll for remote tracking of volcanic activity, *Eos Trans. AGU*, *84*(40), 409–424.
Harris, A. J. L., et al. (2005), DUCKS: Low cost thermal monitoring units for near-vent deployment, *J. Volcanol. Geotherm. Res.*, *143*, 335–360.
Hayashi, S., M. Kasahara, K. Tanaka, and H. Hamaguchi (1992), Major elements chemistry of recent eruptive products from Nyamuragira volcano, Africa (1976–1989), in *Geophysical Study on the Hotspot Volcanoes in the African Continent*, edited by H. Hamaguchi, pp. 83–87, Fac. of Sci., Tohoku Univ., Sendai, Japan.
Herring, T. A., R. W. King, and S. C. McClusky (2010), *Introduction to GAMIT/GLOBK, Release 10.4*, pp. 1–48, MIT Press, Cambridge.
INGV-OE Internal Report (2012a), BollettinoEtna20120508, *Rep. 19/2012*, Catania, Italy. [Available at www.ct.ingv.it.]
INGV-OE Internal Report (2012b), BollettinoEtna20120814, *Rep. 33/2012*, Catania, Italy. [Available at www.ct.ingv.it.]
INGV-OE Internal Report (2012c), BollettinoEtna20120731, *Rep. 31/2012*, Catania, Italy. [Available at www.ct.ingv.it.]
INGV-OE Internal Report (2012d), BollettinoEtna20120904, *Rep. 36/2012*, Catania, Italy. [Available at www.ct.ingv.it.]
INGV-OE Internal Report (2012e), BollettinoEtna20121127, *Rep. 48/2012*, Catania, Italy. [Available at www.ct.ingv.it.]
INGV-OE Internal Report (2012f), BollettinoEtna20121204, *Rep. 49/2012*, Catania, Italy. [Available at www.ct.ingv.it.]
INGV-OE Internal Report (2012g), BollettinoEtna20121218, *Rep. 51/2012*, Catania, Italy. [Available at www.ct.ingv.it.]
INGV-OE Internal Report (2012h), BollettinoEtna20120710, *Rep. 28/2012*, Catania, Italy. [Available at www.ct.ingv.it.]
INGV-OE Internal Report (2012i), BollettinoEtna20121009, *Rep. 41/2012*, Catania, Italy. [Available at www.ct.ingv.it.]
INGV-OE Internal Report (2012j), BollettinoEtna20121023, *Rep. 43/2012*, Catania, Italy. [Available at www.ct.ingv.it.]
INGV-OE Internal Report (2013a), BollettinoEtna20130101, *Rep. 01/2013*, Catania, Italy. [Available at www.ct.ingv.it.]
INGV-OE Internal Report (2013b), BollettinoEtna20130122, *Rep. 04/2013*, Catania, Italy. [Available at www.ct.ingv.it.]
INGV-OE Internal Report (2013c), BollettinoEtna20130129, *Rep. 05/2013*, Catania, Italy. [Available at www.ct.ingv.it.]
INGV-OE Internal Report (2013d), BollettinoEtna20130205, *Rep.06/2013*, Catania, Italy. [Available at www.ct.ingv.it.]
INGV-OE Internal Report (2013e), BollettinoEtna20130212, *Rep. 07/2013*, Catania, Italy. [Available at www.ct.ingv.it.]
INGV-OE Internal Report (2013f), BollettinoEtna20130219, *Rep. 08/2013*, Catania, Italy. [Available at www.ct.ingv.it.]
INGV-OE Internal Report (2013g), BollettinoEtna20130226, *Rep. 09/2013*, Catania, Italy. [Available at www.ct.ingv.it.]
INGV-OE Internal Report (2013h), BollettinoEtna20130305, *Rep. 10/2013*, Catania, Italy. [Available at www.ct.ingv.it.]
INGV-OE Internal Report (2013i), BollettinoEtna20130108, *Rep. 02/2013*, Catania, Italy. [Available at www.ct.ingv.it.]
Jaupart, C., and S. Vergniolle (1988), Laboratory models of Hawaiian and Strombolian eruptions, *Nature*, *331*, 58–60.
Jaupart, C., and S. Vergniolle (1989), The generation and collapse of a foam layer at the roof of a basaltic magma chamber, *J. Fluid Mech.*, *203*, 347–380.
Johnson, J. B., and R. C. Aster (2005), Relative partitioning of acoustic and seismic energy during Strombolian eruptions, *J. Volcanol. Geotherm. Res.*, *148*, 334–354, doi:10.1016/j.jvolgeores.2005.05.002.
Kumagai, H., M. Nakano, T. Maeda, H. Yepes, P. Palacios, M. Ruiz, S. Arrais, M. Vaca, I. Molina, and T. Yamashima (2010), Broadband seismic monitoring of active volcanoes using deterministic and stochastic approaches, *J. Geophys. Res.*, *115*, B08303, doi:10.1029/2009JB006889.
Kumagai, H., T. Saito, G. O'brien, and T. Yamashina (2011), Characterization of scattered seismic wavefields simulated in heterogeneous media with topography, *J. Geophys. Res.*, *116*, B03308, doi:10.1029/2010JB007718.
La Delfa, S., G. Patanè, R. Cliocchiatti, J-L. Joron, and J-C. Tanguy (2001), Activity of Mount Etna preceding the February 1999 fissure eruption: Inferred mechanism from seismological and geochemical data, *J. Volcanol. Geotherm. Res.*, *105*, 121–139.
Langer, H., S. Falsaperla, M. Masotti, R. Campanini, S. Spampinato, and A. Messina (2009), Synopsis of supervised and unsupervised pattern classification techniques applied to volcanic tremor data at Mt Etna, Italy, *Geophys. J. Int.*, *178*(2), 1132–1144.
La Spina, A., and G. Salerno (2009), Composizione del gas emesso dalla bocca apertasi il 6 Novembre 2009 alla base del cratere di Sud-Est, INGV report, *Prot. Int. UFVG2009/88*, Catania, Italy. [Available at www.ct.ingv.it.]
La Spina, A., M. Burton, and G. G. Salerno (2010), Unravelling the processes controlling gas emissions from the central and northeast craters of Mt. Etna, *J. Volcanol. Geotherm. Res.*, *198*, 368–376.
La Spina, A., M. Burton, P. Allard, S. Alparone, and F. Muré (2015), Open-path FTIR spectroscopy of magma degassing processes during eight lava fountains on Mount Etna, *Earth Planet. Sci. Lett.*, *413*, 123–134, doi:10.1016/j.epsl.2014.12.038.
Lisowski, M., D. Dzurisin, R. P. Denlinger, and E. Y. Iwatsubo (2008), Analysis of GPS-measured deformation associated with the 2004-2006 dome-building eruption of Mount St. Helens, Washington, in *A Volcano Rekindled: The Renewed Eruption of Mount St. Helens*, *2004–2006*, *U.S. Geol. Surv., Prof. Pap.*, *1750*, edited by D. R. Sherrod, W. E. Scott, and P. H. Stauffer, chap. 15, pp. 301–333, U.S. Geol. Surv., Reston, Va.
Mangan, M. T., and K. V. Cashman (1996), The structure of basaltic scoria and reticulate and inferences for vesciculation, foam formation, and fragmentation in lava fountains, *J. Volcanol. Geotherm. Res.*, *73*(1-2), 1–18.
Marchetti, E., M. Ripepe, A. J. L. Harris, and D. Delle Donne (2009), Tracing the differences between Vulcanian and Strombolian explosions using infrasonic and thermal radiation energy, *Earth Planet. Sci. Lett.*, *279*, 273–281, doi:10.1016/j.epsl.2009.01.004.
Matoza, R. S., D. Fee, T. B. Neilsen, K. L. Gee, and D. E. Ogden (2013), Aeroacoustics of volcanic jets: Acoustic power estimation and jet velocity dependence, *J. Geophys. Res. Solid Earth*, *118*, 6269–6284, doi:10.1002/2013JB010303.
McNutt, S. R., G. Thompson, M. E. West, D. Fee, S. Stihler, and E. Clark (2013), Local seismic and infrasound observations of the 2009 explosive eruptions of Redoubt Volcano, Alaska, *J. Volcanol. Geotherm. Res.*, *259*, 63–76, doi:10.1016/j.jvolgeores.2013.03.016.
Merucci, L., M. Burton, S. Corradini, and G. G. Salerno (2011), Reconstruction of SO_2 flux emission chronology from space-based measurements, *J. Volcanol. Geotherm. Res.*, *206*, 80–87.
Métrich, N., R. Cocchiatti, M. Mosbash, and M. Chaussidon (1993), The 1989–1990 activity of Etna: Magma mingling and ascent of H_2O-Cl-S-rich basaltic magma. Evidence from melt inclusions, *J. Volcanol. Geotherm. Res.*, *59*, 131–140.

Mogi, K. (1958), Relations between the eruptions of various volcanoes and the deformations of the ground surfaces around them, *Bull. Earthquake Res. Inst. Univ. Tokyo*, *36*, 99–134.
Montgomery-Brown, E. K., D. K. Sinnett, K. M. Larson, M. P. Poland, P. Segall, and A. Miklius (2011), Spatiotemporal evolution of dike opening and décollement slip at Kīlauea Volcano, Hawai'i, *J. Geophys. Res.*, *116*, B03401, doi:10.1029/2010JB007762.
Morè, J. J. (1977), The Levenberg-Marquardt algorithm: Implementation and theory, in *Numerical Analysis, Lecture Notes Math. 630*, edited by G. A. Watson, pp. 105–116, Springer, Berlin, doi:10.1007/BFb0067700.
Mulargia, F., S. Tinti, and E. Boschi (1985), A statistical analysis of flank eruptions on Etna volcano, *J. Volcanol. Geotherm. Res.*, *23*, 263–272.
Murè, F., G. Larocca, L. Spampinato, T. Caltabiano, G. G. Salerno, P. Montalto, and L. Scuderi (2013), Installazione di un radiometro nell'area sommitale del vulcano Etna, *Rapp. Tecnici INGV*, *259*, Istit. Naz. di Geofis. e Vulcanol., Catania, Italy.
Oppenheimer, C., and P. Francis (1997), Remote sensing of heat, lava and fumarole emissions from Erta 'Ale volcano, Ethiopia, *Int. J. Remote Sens.*, *18*(8), 1661–1692.
Oppenheimer, C., P. W. Francis, D. A. Rothery, R. W. T. Carlton, and L. S. Glaze (1993), Infrared image analysis of volcanic thermal features: Láscar Volcano, Chile, 1984–1992, *J. Geophys. Res.*, *98*(B3), 4269–4286.
Oppenheimer, C., D. M. Pyle, and J. Barcaly (2003), *Volcanic Degassing,. Geol. Soc. Spec. Publ.*, *213*, pp. 420, Geol. Soc. of London, London, U. K.
Oppenheimer, C., T. O. Fischer, and B. Scaillet (2014), Volcanic degassing: Process and impact, in *Treatise on Geochemistry*, vol. 4, 2nd ed., edited by H. D. Holland and K. K. Turekian, pp. 111–179, Elsevier, Oxford, U. K.
Palano, M., G. Puglisi, and S. Gresta (2008), Ground deformation patterns at Mt. Etna from 1993 to 2000 from joint use of InSAR and GPS techniques, *J. Volcanol. Geotherm. Res.*, *169*(3-4), 99–120, doi:10.1016/j.jvolgeores.2007.08.014.
Palano, M., M. Rossi, C. Cannavò, V. Bruno, M. Aloisi, D. Pellegrino, M. Pulvirenti, G. Siligato, and M. Mattia (2010), Etn@ref, a geodetic reference frame for Mt. Etna GPS networks, *Ann. Geophys.*, *53*(4), 48–79, doi:10.4401/af-4879.
Parfitt, E. A. (1998), A study of clast size distribution, ash deposition and fragmentation in a Hawaiian-style volcanic eruption, *J. Volcanol. Geotherm. Res.*, *84*, 197–208.
Parfitt, E. A. (2004), A discussion of the mechanisms of explosive basaltic eruptions, *J. Volcanol. Geotherm. Res.*, *134*, 77–107.
Patanè, D., G. Di Grazia, A. Cannata, P. Montalto, and E. Boschi (2008), The shallow magma pathway geometry at Mt. Etna volcano, *Geochem. Geophys. Geosyst.*, *9*, Q12021, doi:10.1029/2008GC002131.
Patanè, D., et al. (2013), Insights into magma and fluid transfer at Mount Etna by a multiparametric approach: A model of the events leading to the 2011 eruptive cycle, *J. Geophys. Res. Solid Earth*, *118*, 1–21, doi:10.1002/jgrb.50248.
Peltier, A., T. Staudacher, and P. Bachèlery (2010), New behaviour of the Piton de La Fournaise volcano feeding system (La Réunion Island) deduced from GPS data: Influence of the 2007 Dolomieu caldera collapse, *J. Volcanol. Geotherm. Res.*, *192*, 48–56, doi:10.1016/j.jvolgeores.2010.02.007.
Platt, U., and J. Stutz (2008), *Differential Optical Absorption Spectroscopy Principles and Applications, Phys. Earth Space Environ*., 597 pp., Springer, Berlin.
Richardson, J. P., G. P. Waite, and J. L. Palma (2014), Varying seismic-acoustic properties of the fluctuating lava lake at Villarica volcano, Chile, *J. Geophys. Res. Solid Earth*, *119*, 5560–5573, doi:10.1002/2014JB011002.
Rittmann, A. (1973), Structure and evolution of Mount Etna, *Philos. Trans. R. Soc. London A*, *274*, 5–16.
Rodgers, C. (2000), *Inverse Methods for Atmospheric Sounding, Theory and Practice, Ser. Atmos. Oceanic Planet. Phys*., vol. 2, World Sci., Singapore.
Sahetapy-Engel, S. T., A. J. L. Harris, and E. Marchetti (2008), Thermal, seismic and infrasound observations of persistent explosive activity and conduit dynamics at santiaguito lava dome, Guatemala, *J. Volcanol. Geotherm. Res.*, *173*, 1–14.
Salerno, G. G., M. Burton, C. Oppenheimer, T. Caltabiano, V. I. Tsanev, and N. Bruno (2009a), Novel retrieval of volcanic SO_2 abundance from ultraviolet spectra, *J. Volcanol. Geotherm. Res.*, *181*, 141–153.
Salerno, G. G., M. R. Burton, C. Oppenheimer, T. Caltabiano, D. Randazzo, N. Bruno, and V. Longo (2009b), Three-years of SO_2 flux measurements of Mt. Etna using an automated UV scanner array: Comparison with conventional traverses and uncertainties in flux retrieval, *J. Volcanol. Geotherm. Res.*, *183*, 76–83.
Sciotto, M., A. Cannata, G. Di Grazia, S. Gresta, E. Privitera, and L. Spina (2011), Seismoacoustic investigations of paroxysmal activity at Mt. Etna volcano: New insights into the 16 November 2006 eruption, *J. Geophys. Res.*, *116*, B09301, doi:10.1029/2010JB008138.
Spampinato, L., S. Calvari, C. Oppenheimer, and L. Lodato (2008), Shallow magma transport for the 2002–3 Mt. Etna eruption inferred from thermal infrared surveys, *J. Volcanol. Geotherm. Res.*, *177*, 301–312.
Spampinato, L., S. Calvari, C. Oppenheimer, and E. Boschi (2011), Volcano surveillance using infrared cameras, *Earth Sci. Rev.*, *106*, 63–91.
Spampinato, L., G. Ganci, P. A. Hernández, D. Calvo, D. Tedesco, N. M. Pérez, S. Calvari, C. Del Negro, and M. M. Yalire (2013), Thermal insights into the dynamics of Nyiragongo lava lake from ground and satellite measurements, *J. Geophys. Res. Solid Earth*, *118*, 5771–5784, doi:10.1002/2013JB010520.
Spilliaert, N., N. Métrich, and P. Allard (2006), S–Cl–F degassing pattern of water-rich alkali basalt: Modelling and relationship with eruption styles on Mount Etna volcano, *Earth Planet. Sci. Lett.*, *248*, 772–786.
Staudacher, T., V. Ferrazzini, A. Peltier, P. Kowalski, P. Boisser, P. Catherine, P., F. Lauret, and F. Massin (2009), The April 2007 eruption and the Dolomieu crater collapse, two major events at Piton de la Furnaces (La Réunion Island, Indian Ocean), *J. Volcanol. Geotherm. Res.*, *184*(1–2), 126–137.
Stovall, W. K., B. F. Houghton, H. Gonnermann, S. A. Fagents, and D. A. Swanson (2011), Eruption dynamics of Hawaiian-style fountains: The case study of episode 1 of the Kīlauea Iki 1959 eruption, *Bull. Volcanol.*, *73*(5), 511–529.
Tait, S. R., C. Jaupart, and S. Vergniolle (1989), Pressure, gas content and eruption periodicity of a shallow crystallising magma chamber, *Earth Planet. Sci. Lett.*, *92*, 107–123.
Tiampo, K. F., J. B. Rundle, J. Fernandez, and J. O. Langbein (2000), Spherical and ellipsoidal volcanic sources at Long Valley caldera, California using a genetic algorithm inversion technique, *J. Volcanol. Geotherm. Res.*, *102*(3), 189–206.
Vergniolle, S., and Y. Gaudemer (2012), Decadal evolution of a degassing magma reservoir unraveled from fire fountains produced at Etna volcano (Italy) between 1989 and 2001, *Bull. Volcanol.*, *74*, 725–742.
Vergniolle, S., and M. Ripepe (2008), From Strombolian explosions to fire fountains at Etna Volcano (Italy): What do we learn from acoustic measurements, *Geol. Soc. Spec. Publ.*, *307*, 103–124.
Vergniolle, S., M. Boichu, and J. Caplan-Auerbach (2004), Acoustic measurements of the 1999 basaltic eruption of Shishaldin volcano, Alaska: 1. Origin of Strombolian activity, *J. Volcanol. Geotherm. Res.*, *137*, 109–134.

West, M. E. (2013), Recent eruptions at Bezymianny volcano—A seismological comparison, *J. Volcanol. Geotherm. Res.*, *263*, 42–57, doi: 10.1016/j.jvolgeores.2012.12.015.

Williams, C. A., and G. Wadge (2000), An accurate and efficient method for including the effects of topography in three-dimensional elastic models of ground deformation with applications to radar interferometry, *J. Geophys. Res.*, *105*(B4), 8103–8120, doi:10.1029/1999JB900307.

Williams-Jones, G., J. Stix, and C. Hickson (2008), *The COSPEC Cookbook: Making SO2 Measurements at Active Volcanoes, Methods Volcanol.*, vol. 1, pp. 233, Int. Assoc. of Volcnol. Chem. Earth Inter.

Wilson, L., and J. W. Head (1981), Ascent and eruption of basaltic magma on the Earth and Moon, *J. Geophys. Res.*, *86*(B4), 2971–3001.

Wilson, L., and J. W. Head (2001), Lava fountains from the 1999 Tvashtar Catena fissure eruption on Io: Implications for dike emplacement mechanisms, eruption rates, and crustal structure, *J. Geophys. Res.*, *106*(E12), 32,997–33,004.

Yang, X. M., P. M. Davis, and J. H. Dieterich (1988), Deformation from inflation of a dipping finite prolate spheroid in an elastic half-space as a model for volcanic stressing, *J. Geophys. Res.*, *93*(B5), 4249–4257, doi:10.1029/JB093iB05p04249.